Quantum chaos in a system with high degree of symmetries

Javier de la Cruz,[1] Sergio Lerma-Hernández,[2] and Jorge G. Hirsch[1]
[1]*Instituto de Ciencias Nucleares, Universidad Nacional Autónoma de México, Apdo. Postal 70-543, C.P. 04510 Cd. Mx., Mexico*
[2]*Facultad de Física, Universidad Veracruzana, Circuito Aguirre Beltrán s/n, Xalapa, Veracruz 91000, Mexico*

(Received 13 May 2020; accepted 18 August 2020; published 8 September 2020)

We study dynamical signatures of quantum chaos in one of the most relevant models in many-body quantum mechanics, the Bose-Hubbard model, whose high degree of symmetries yields a large number of invariant subspaces and degenerate energy levels. The standard procedure to reveal signatures of quantum chaos requires classifying the energy levels according to their symmetries, which may be experimentally and theoretically challenging. We show that this classification is not necessary to observe manifestations of spectral correlations in the temporal evolution of the survival probability, which makes this quantity a powerful tool in the identification of chaotic many-body quantum systems.

DOI: 10.1103/PhysRevE.102.032208

I. INTRODUCTION

Symmetries play an important role in the description of physical systems, helping to simplify their description and temporal evolution. In classical dynamics they are useful to find the coordinates providing the simplest description, and in the many-body quantum domain they allow us to divide the Hilbert space in unconnected subspaces, strongly reducing the dimensionality of the problem. Degeneration of energy levels is rare in Hamiltonian systems, usually reflecting the existence of symmetries in them [1,2].

Quantum chaos refers to quantum signatures of classically chaotic systems and their universal properties associated with random matrix theory. In the presence of these properties, quantum systems with no classical analogues are also referred to as chaotic quantum systems [2–4]. Among quantum chaos diagnoses, one of the most popular is spectral statistics, which requires the classification of the levels by their symmetry properties [5–7]. In systems with many symmetries, this process can be very demanding on the theoretical side, and very difficult to implement in experimental studies. For example, in the Bose-Hubbard model (BHM), which is the system that we analyze here, the number of symmetry subspaces is at least as large as the number of sites in the lattice.

The BHM is the simplest description of a set of spin-less bosons with onsite interactions in a lattice. It was the first strongly correlated lattice model being realized with ultracold atoms and in which a quantum phase transition was observed [8]. Due to the high degree of controllability and new observational tools, which enable the detection of each individual atom, the model is employed to describe experimental quantum simulations, quantum thermalization and in recent years quantum virtual cooling [9–14].

The spectral properties associated with quantum chaos in the BHM were studied by Kolovsky and Buchleitner [15]. Lubasch studied measures to explore the relation between quantum chaos and entanglement [16]. Semiclassical analysis connected with interfering paths in Fock space were presented in Ref. [17], with periodic mean field solutions in [18] and with Bloch oscillations in Ref. [19]. The out-of-time-order correlator (OTOC) and the Lyapunov exponent have also been studied [20] and the statistical distance between initially similar number distributions has been proposed as a reliable measure to distinguish regular from chaotic behavior in a Bose-Hubbard dimer [21]. Recently the half-chain entanglement entropy has been used like an indicator of ergodicity breaking in the clean Bose-Hubbard chain [22].

In the present work we use the survival probability, a dynamical observable, to identify quantum chaos in the BHM. The survival probability is the probability to find the system in its initial state at time t. In chaotic systems, it exhibits a correlation hole of universal character at long times. This corresponds to a dip below the saturation value of the dynamics reached at even longer times. The correlation hole was proposed in Ref. [23] as a way to detect level repulsion in molecules [24–26], where the experimental line resolution is not as good as in nuclear physics. The idea was that, even if the experiment would miss some of the lines, the hole would still indicate if the eigenvalues were correlated or not. It can be described analytically employing the two-level form factor of random matrix theory [27–30], exhibiting thus the relevance of random matrices as models for the dynamics of quantum systems that are chaotic in the classical limit [31]. This observable has been successfully employed as a quantum chaos indicator in recent works in spin systems [32–36] and in atom-photon systems [37].

Here we show that, contrary to spectral statistics where the signatures of quantum chaos disappear when many symmetry sectors are considered together, in the survival probability the correlation hole manifests even if the whole set of symmetry sectors are included in the dynamics. When all the symmetry sectors are considered, the distribution of the spacings of neighboring energy levels changes from Wigner-Dyson to

Poisson, whereas the correlation hole in the survival probability is still clearly seen. Analytical expressions are provided, which, besides giving theoretical support to the persistence of the correlation hole, describe the complete evolution of the survival probability, both in the case of one and several symmetry subspaces.

A drawback of the survival probability is its lack of self-averaging at any time scale, that is the relative variance of its fluctuations does not decrease with system size [35,38,39]. For this reason, ensemble averages over an energy window [37] or averages over initial states [40] are required to make the correlation hole visible. Any of the two options are experimentally accessible.

The structure of the paper is as follows. In Sec. II we introduce the BHM, its symmetries and the properties of its energy spectrum. Then we describe the dynamics of the survival probability and the correlation hole in Sec. III, both in the case of one symmetry sector and when the whole set of invariant subspaces is considered together. In Sec. IV, the analytical expressions derived in the previous section are shown to describe properly numerical results for the BHM in a chaotic regime. The way these signatures of quantum chaos disappear as we move to integrable limits is also discussed. To finish, our conclusions are given in Sec. V.

II. THE BOSE-HUBBARD MODEL

The model which we consider is the one-dimensional BHM with periodic boundary conditions. This model describes N spin-less bosons on a lattice with L sites in a ring array, relevant to numerous experiments with cold atoms in optical lattices. The Hamiltonian of this system, with $\hbar = 1$, is

$$\hat{H} = -J \sum_{l=1}^{L} \left(\hat{a}_{l+1}^{\dagger}\hat{a}_l + \text{H.c.}\right) + \frac{U}{2}\sum_{l=1}^{L} \hat{n}_l(\hat{n}_l - 1). \quad (1)$$

The operators $\hat{a}_l^{\dagger}$ and $\hat{a}_l$ are the creation and annihilation operators of one boson on the site l, respectively. Due to periodic boundary conditions, the index $L+1$ in the first sum should be considered as $L+1 := 1$. The first term is the kinetic energy, describing the coherent tunneling between adjacent sites with rate J. The second term describes the interaction energy on-site with intensity U, where $\hat{n}_l = \hat{a}_l^{\dagger}\hat{a}_l$ gives the number of particles on site l and the total number of particles is constant, $\sum_{l=1}^{L} \hat{n}_l = N$.

One of the most relevant aspects of the system is that in the thermodynamic limit it presents a second order quantum phase transition, going from a Mott insulator to a superfluid phase [8,41,42].

A. Symmetries and degenerated subspaces

The symmetries of the BHM are described by the dihedrical group D_L, which is the group of symmetries of a regular polygon with L sides. One of the symmetries is related to the translational invariance of the Hamiltonian due to the periodic boundary conditions. The shift operator $\hat{S}$ is responsible for the decomposition into different κ-subspaces and acts in a Fock state as

$$\hat{S}\,|n_1, n_2, ..., n_{L-1}, n_L\rangle = |n_L, n_1, n_2, ..., n_{L-1}\rangle\,. \quad (2)$$

The eigenvalues of $\hat{S}$ are $a_j = e^{i\kappa_j}$ with $\kappa_j = 2\pi j/L$, the single particle quasimomentum and $j = 1, 2, ..., L$ [19]. The only other symmetry is the parity, which is defined as

$$\hat{\mathcal{P}}\,|n_1, n_2, ..., n_{L-1}, n_L\rangle = |n_L, n_{L-1}, ..., n_2, n_1\rangle. \quad (3)$$

The shift and the parity operators commute with the BH Hamiltonian Eq. (1). However $[\hat{S}, \hat{\mathcal{P}}] \neq 0$, which entails a pairwise degenerate spectrum between states belonging to the subspaces with eigenvalues a_j and $a_j^* = a_{L-j}$. For $a_{j=L} = 1$ or $a_{j=L/2} = -1$ (the latter appearing only for L even) the subspaces can be decomposed in two additional subspaces with definite parity. In this way we can classify the entire Hamiltonian spectrum.

Fig. 1(a) shows a schematic representation of the shift and parity operator acting on a system of $L = 9$ sites. From now on, we consider this number of sites and the same number of bosons $N = 9$. For this choice, the Hilbert space dimension is $\mathcal{D} = 24310$, and it can be decomposed into 9 subspaces associated with the eigenvalues a_j of $\hat{S}$ as shown in the Fig. 1(b). The dimensions of the subspaces are $\mathcal{D}_1 = \mathcal{D}_8 = 2700$, $\mathcal{D}_2 = \mathcal{D}_7 = 2700$, $\mathcal{D}_3 = \mathcal{D}_6 = 2703$, $\mathcal{D}_4 = \mathcal{D}_5 = 2700$, $\mathcal{D}_9 = 2704$. Additionally, the subspace associated with $j = 9$ can be decomposed in two subspaces with definite parity, whose dimensions are $\mathcal{D}_{9\text{-even}} = 1387$ and $\mathcal{D}_{9\text{-odd}} = 1317$. In Fig. 1(b) each subspace pair related by a black arrow has the same spectrum. Only the 9-subspace has no degeneracies, and the two subspaces with different parity have different spectrum. This is the full decomposition of the system in symmetries.

For the Hamiltonian parameters, we use the parametrization introduced in Ref. [43] $U = u$ and $J = 1 - u$ with $u \in [0, 1]$. With this parametrization the system is integrable in the two limits $u = 0$ and $u = 1$. Except for some few indicated cases, in the following sections we use the value $u = 0.5$ as a representative chaotic example.

B. Level statistics and density of states

We obtained the full spectrum of the model by exact numerical diagonalization. The density of states (DoS) $\nu(E)$ is shown in the Fig. 2(a). The DoS has a Gaussian form, common in many body interacting systems with a finite Hilbert space. Due to the similar dimension of the subspaces the density of states in each one is very close to a ninth of the total density of states $\nu_j(E) = \nu(E)/9$, for $j = 1, ..., 9$. The light gray zone in Fig. 2(a) depicts the energy interval that we consider in the numerical calculations presented below for the spectral distributions and the survival probability. This is a window of width equal to four (energy units) with center in the maximum of the distribution.

The nearest-neighbor spacing distribution for the unfolded energy levels of the 1-subspace, containing the central 80% of its spectrum, is shown in Fig. 2(b). The red-dashed line is the Wigner-Dyson distribution for the Gaussian orthogonal ensemble (GOE). We have verified the same very good match with the Wigner-Dyson distribution for the energy spacing of the other symmetry subspaces.

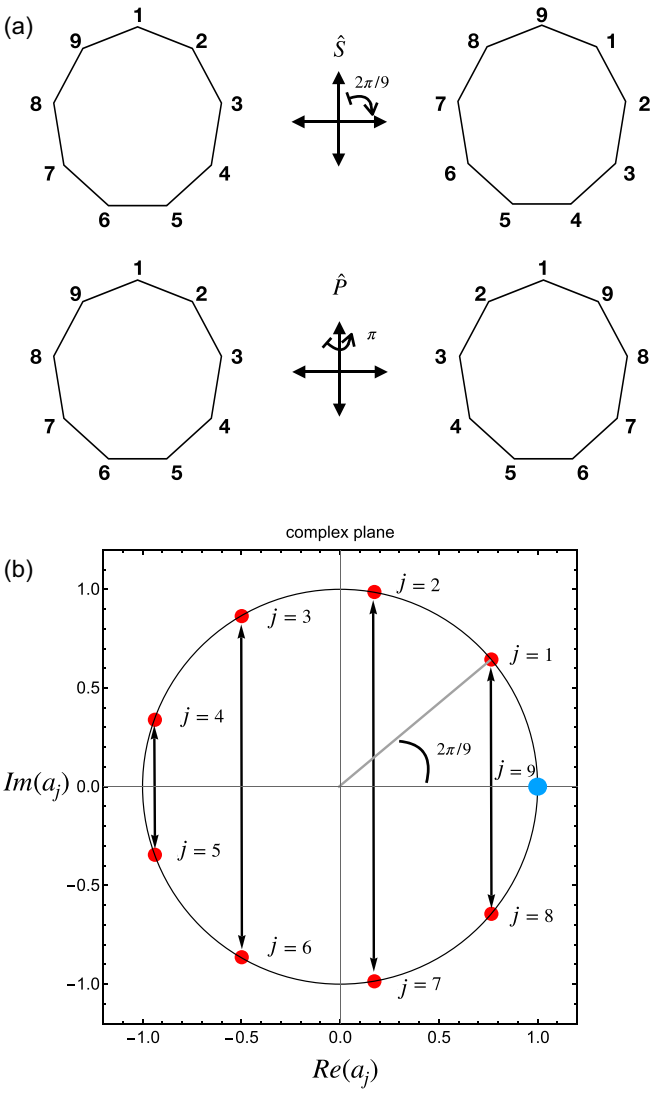

FIG. 1. (a) Schematic representations of the shift $\hat{S}$ and parity $\hat{\mathcal{P}}$ operators. These operators describe the symmetries of the BH model with periodic boundary conditions and are the same as those of a regular polygon of L sides. (b) Eigenvalues of $\hat{S}$ in the complex plane, for $L = 9$ sites, indicated by dots. Pairwise subspaces related by complex conjugate eigenvalues of $\hat{S}$ have the same spectrum, these are linked by the black arrows. The subspace $j = 9$ is the only nondegenerate subspace and it has two parity symmetric invariant subspaces.

If instead we consider all the energy levels in the interval in the middle of the spectrum, as indicated in Fig. 2(a), and do not separate them by symmetry sectors, then we obtain the unfolded energy spacing distribution displayed in the inset of Fig. 3. The distribution shows a peak at zero energy, which comes from the exact respective degeneracies between subspaces $j = 1$–4 and $j = 8$–5. If we remove these exact degeneracies by considering only subspaces $j = 1$–4 and $j = 9$, then we get rid of the peak and obtain a distribution very close to a Poisson distribution of uncorrelated levels, as can be seen in the main panel of Fig. 3. This well known result shows that the nearest-neighbor distribution is unable, when

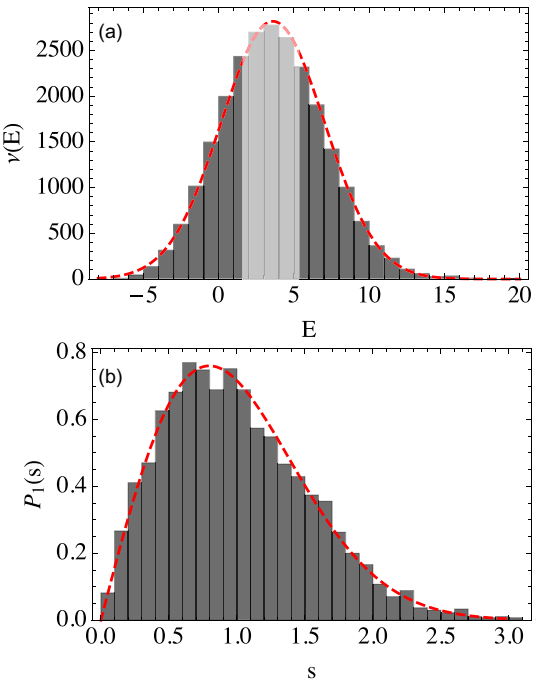

FIG. 2. (a) Gray bars depict the density of states (DoS) obtained numerically for the BHM with $L = 9$ sites and $N = 9$ bosons, for $u = 0.5$. A Gaussian fit is shown by the red dashed line. The light-gray zone in the DoS represents the energy interval used in panel (b) and Figs. 3, 4, and 7 (top). (b) Nearest-neighbour level spacing distribution for the unfolded spectrum of the subspace associated to the $j = 1$ ($\kappa_1 = 2\pi/9$) symmetry subspace. The distribution coincides with the Wigner-Dyson surmise of the GOE ensemble (dashed red line).

the energy eigenstates belonging to different symmetry sectors are considered together, to reflect the repulsion between levels within the same symmetry sector. These correlations become hidden by the lack of correlations between levels with different symmetries.

As we show below, this is not the case of the survival probability, which is sensitive to the correlations in the spectrum even if several symmetry sectors are considered together. In what follows we discuss how these correlations manifest as

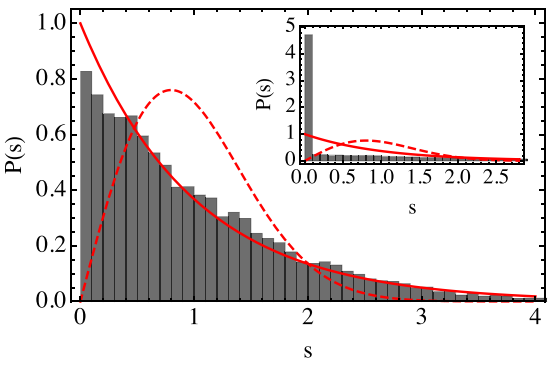

FIG. 3. Main panel shows the nearest-neighbor spacing distribution of energy levels in the light gray region of Fig. 2 considering subspaces $j = 1 - 4$ and $j = 9$. Inset shows the same distribution for the whole set of symmetry subspaces.

a dip in the temporal evolution of the survival probability, known as correlation hole, and compare it with the spectral analysis performed above.

III. THE SURVIVAL PROBABILITY AND THE CORRELATION HOLE

The survival probability is a dynamical observable defined as the probability to find a given initial state $|\Psi(0)\rangle$ at time t,

$$S_P(t) = |\langle\Psi(0)|\Psi(t)\rangle|^2. \tag{4}$$

If we expand the initial state $|\Psi(0)\rangle$ in the energy eigenbasis $\{|\phi_k\rangle\}$,

$$|\Psi(0)\rangle = \sum_{k=1}^{\mathcal{D}} c_k\,|\phi_k\rangle\,, \tag{5}$$

where $\hat{H}\,|\phi_k\rangle = E_k\,|\phi_k\rangle$ and $c_k = \langle\phi_k|\Psi(0)\rangle$, then the survival probability reads

$$S_P(t) = \left|\sum_k |c_k|^2 e^{-iE_k t}\right|^2. \tag{6}$$

A. Initial decay and asymptotic value

The survival probability can be expressed as the squared modulus of the Fourier transform of the local density of states (LDOS)

$$S_P(t) = \left|\int \mathcal{G}(E)e^{-iEt}dE\right|^2, \tag{7}$$

where the LDOS, $\mathcal{G}(E) = \sum_k |c_k|^2\delta(E - E_k)$, is the energy distribution weighted by the components of the initial state. By considering a smooth approximation to the LDOS, $\rho(E) \approx \mathcal{G}(E)$, we can obtain an analytical expression for the initial decay of $S_P(t)$ [32,37]. For instance, for a smoothed LDOS described by a rectangular profile,

$$\rho(E) = \begin{cases} \frac{1}{2\sigma_R} & \text{for } E \in [E_c - \sigma_R, E_c + \sigma_R] \\ 0 & \text{otherwise} \end{cases}, \tag{8}$$

we obtain a sin$c$ squared function for the initial decay of $S_P(t)$

$$S_p^{bc}(t) = \frac{\sin^2(\sigma_R t)}{(\sigma_R t)^2}, \tag{9}$$

where the super-index bc indicates that this expression is valid before the dynamics is able to resolve the correlations in the spectrum. In the following, we consider this rectangular energy profile with parameters determined by the energy window of Fig. 2, where $E_c = 3.60$ is the center of the distribution and $\sigma_R = 2$ is its half-width.

The initial decay holds up to a temporal scale where the dynamics is able to resolve the discrete nature of the energy spectrum. For $t \to \infty$, the survival probability fluctuates around an asymptotic value, S_P^∞, which can be determined as follows. By expanding the squared modulus in Eq. (6), we obtain

$$S_P(t) = \sum_{k\neq l} |c_l|^2|c_k|^2 e^{-i(E_k - E_l)t} + \sum_k |c_k|^4. \tag{10}$$

The asymptotic value can be obtained by considering a temporal average of this expression

$$S_P^\infty = \lim_{t\to\infty} \frac{1}{t}\int_0^\infty S_P(t')dt'. \tag{11}$$

In the absence of degeneracies, the first term in the right-hand side (RHS) of Eq. (10) cancels out in average and

$$S_P^\infty = \sum_k |c_k|^4, \tag{12}$$

which is the case of the BHM when only one symmetry sector is considered. In the case of degeneracies, that appear in the BHM when several symmetry sectors are considered, the first term in the RHS of Eq. (10) contributes with extra terms to the asymptotic value, which is now given by

$$S_P^\infty = \sum_{E_k}\left(\sum_{m=1}^{d_{E_k}} \left|c_{E_k,m}\right|^2\right)^2, \tag{13}$$

where $c_{E_k,m}$ is the component of the initial state in the energy level $|E_k, m\rangle$ with degeneracy d_{E_k},

$$c_{E_k,m} = \langle E_k; m|\Psi(0)\rangle \quad (m = 1, ..., d_{E_k}).$$

B. Initial states

In between the initial decay and the saturation of the dynamics, correlations in the energy spectrum manifest as a dip of the S_P below the asymptotic value. To reveal the presence of this correlation hole, averages over different initial states have to be considered [32–37]. On the one hand, this is a necessary step to overcome the quantum fluctuations in the temporal evolution of the survival probability, whose size relative to the average value do not diminish with the size of the system: they are not self-averaging [39]. On the other hand, the preparation of these sets of initial states has been recently realized in trapped ion systems [40].

In this paper we consider ensembles of initial states with components different to zero only in the energy interval $[E_c - \sigma_R, E_c + \sigma_R]$ and whose squared modulus are randomly chosen as follows:

$$|c_k|^2 = \frac{r_k f(E_k)}{\sum_q r_q f(E_q)}, \tag{14}$$

where $r_k \in [0, 1]$ are random numbers coming from a uniform distribution. The function $f(E) = \rho(E)/\nu(E)$ guarantees that the random initial state has the selected energy profile $\rho(E)$ [Eq. (8) in our case]. This is achieved by compensating, with the denominator, for changes in the density of states.

C. Analytical expressions for the survival probability

1. One symmetry sector

In Ref. [37], by following an idea initially introduced in Ref. [34], an analytical expression for the ensemble average of the survival probability was derived, which applies for the case of one sequence of nondegenerate energy levels with energy density ν and correlations similar to those of random

matrices of a Gaussian orthogonal ensemble (GOE),

$$\langle S_P(t)\rangle = \frac{1-\langle S_P^\infty\rangle}{\eta-1}\left[\eta S_P^{bc}(t) - b_2\left(\frac{t}{2\pi\,\bar{\nu}}\right)\right] + \langle S_P^\infty\rangle, \quad (15)$$

here $S_P^{bc}(t)$ is given in Eq. (9), $\bar{\nu}$ is the mean DoS in the energy interval, and η is the effective dimension of energy levels available for the ensemble, which is given by

$$\eta = \frac{1}{\int dE\,\frac{\rho^2(E)}{\nu(E)}} = \frac{4\sigma_R^2}{\int_{E_c-\sigma_R}^{E_c+\sigma_R} dE\,\frac{1}{\nu(E)}}, \quad (16)$$

where in the last equality we have used the rectangular profile for the energy distribution. When the energy interval is approximately centered in the middle of the Gaussian distribution for $\nu(E)$, the last equation can be approximated by substituting $\nu(E)$ in the denominator by its average in the energy interval ($\bar{\nu}$), leading to a simple expression

$$\eta = 2\sigma_r\bar{\nu},$$

which equals the number of states in the energy interval. The asymptotic value $\langle S_P^\infty\rangle$ is obtained by averaging Eq. (12), which can be shown [37] to be given by

$$\langle S_P^\infty\rangle = \frac{\langle r^2\rangle}{\langle r\rangle^2}\frac{1}{\eta} = \frac{4}{3\eta}, \quad (17)$$

where $\langle r^n\rangle$ is the nth moment of the distribution of the random numbers and in the last equality we have used that for a uniform distribution $\langle r^n\rangle = 1/(n+1)$.

The second term inside the brackets in Eq. (15) is the two-level form factor of the GOE ensemble [30],

$$b_2(t) = [1-2t+t\ln(2t+1)]\Theta(1-t) + \left[t\ln\left(\frac{2t+1}{2t-1}\right)-1\right]\Theta(t-1), \quad (18)$$

where Θ is the Heaviside step function. The two-level form factor brings the survival probability from its minimum value up to the asymptotic value $\langle S_P^\infty\rangle$, creating the dip that is known as the *correlation hole*. Although the averaged survival probability can display oscillations, the presence of a hole, which can be described by Eq. (15), is a direct signature of the existence of correlated eigenvalues, and it does not develop in systems with uncorrelated eigenvalues.

2. *Whole set of symmetry sectors*

Equation (15) is applicable to the BHM when only one symmetry sector is considered. Here we extend Eq. (15) to the case where the whole set of symmetry sectors is included. The interesting point is that the correlations between the energy levels coming from the same symmetry sectors are still reflected in the behavior of the ensemble average of the survival probability, which in a very general case is given by (see the Appendix for a detailed derivation)

$$\langle S_P(t)\rangle_a = \frac{\left(1-\frac{\langle r^2\rangle}{\langle r\rangle^2}\frac{1}{\eta}\right)}{\eta-1}\left[\eta S_P^{bc}(t) - \sum_{i=1}^{N_e} d_i^2\frac{\bar{\nu}_i}{\bar{\nu}}b_2\left(\frac{t}{2\pi\,\bar{\nu}_i}\right)\right] + \langle S_P^\infty\rangle_a, \quad (19)$$

where N_e is the number of energy sequences. We assume GOE correlations for energy levels in the same sequence, and no correlations between different sequences. The degeneracy and density of states of each sequence are given, respectively, by d_i and ν_i with $i = 1, ..., N_e$. The density of states of the whole spectrum satisfies $\nu = \sum_i^{N_e} d_i\nu_i$ and η is given by Eq. (16). The energy components of the ensemble's members are still given by Eq. (14), where the random numbers r_k come from a given probability distribution $p(r)$ with momenta $\langle r^k\rangle = \int r^k p(r)dr$. The asymptotic value of the survival probability is obtained by ensemble averaging Eq. (13), which leads to (see the Appendix for details)

$$\langle S_P^\infty\rangle_a = \frac{\langle r^2\rangle}{\langle r\rangle^2}\frac{1}{\eta} + \frac{\left(1-\frac{\langle r^2\rangle}{\langle r\rangle^2}\frac{1}{\eta}\right)}{\eta-1}\sum_{i=1}^{N_e} d_i(d_i-1)\frac{\nu_i}{\nu}. \quad (20)$$

For the BHM with $L = 9$ sites, the twofold degeneracies between sectors κ_j-κ_{L-j} yield $N_e = 6$ different energy sequences whose densities are approximately $\nu_j = \nu/9$ ($j = 1, ..., 4$) and $\nu_{9\text{-even}} = \nu_{9\text{-odd}} = \nu/18$, while their degeneracies are $d_j = 2$ for $j = 1, ..., 4$ and $d_{9\text{-even}} = d_{9\text{-odd}} = 1$. In this case and for random numbers r_k in Eq. (14) coming from a uniform distribution, the ensemble average of the survival probability reads

$$\langle S_P(t)\rangle_a = \frac{1-\frac{4}{3\eta}}{\eta-1}\left[\eta S_P^{bc}(t) - \frac{16b_2\left(\frac{9t}{2\pi\,\bar{\nu}}\right)+b_2\left(\frac{18t}{2\pi\,\bar{\nu}}\right)}{9}\right] + \langle S_P^\infty\rangle_a, \quad (21)$$

with the asymptotic value $\langle S_P^\infty\rangle_a$,

$$\langle S_P^\infty\rangle_a = \frac{4}{3\eta} + \frac{8}{9}\frac{\left(1-\frac{4}{3\eta}\right)}{\eta-1} \xrightarrow{\eta\gg1} \frac{20}{9\eta}. \quad (22)$$

As already mentioned, the key point is that, again, as in the case of only one symmetry sector, the intracorrelations of levels in the same symmetry sectors, brings the survival from its minimum up to the asymptotic value, creating a correlation hole.

At variance with the one-symmetry case, in this case the correlation hole is governed by a pair of two-level form-factors b_2. One coming from the subspaces $j = 1$–8 which implies that the density entering in its argument is $\bar{\nu}_j = \bar{\nu}/9$, while the second comes from intra-correlations in the spectrum of subspaces 9-even and 9-odd. That is why in the argument of this b_2 function enters $\bar{\nu}_{9\text{-even}} = \bar{\nu}_{9\text{-odd}} = \bar{\nu}/18$. Since the dynamics of subspaces $j = 1$–8 have the same temporal scale, their individual contributions add coherently to build up the correlation hole and they dominate the second term inside the parenthesis in Eq. (21).

IV. NUMERICAL VERSUS ANALYTICAL RESULTS

In this section we compare the analytical expressions for the survival probability from the previous section with numerical results obtained by diagonalizing numerically the BHM for one and the whole set of symmetry sectors. We also study the way the correlation hole, signaling the presence of chaos, dilutes as we approach an integrable limit.

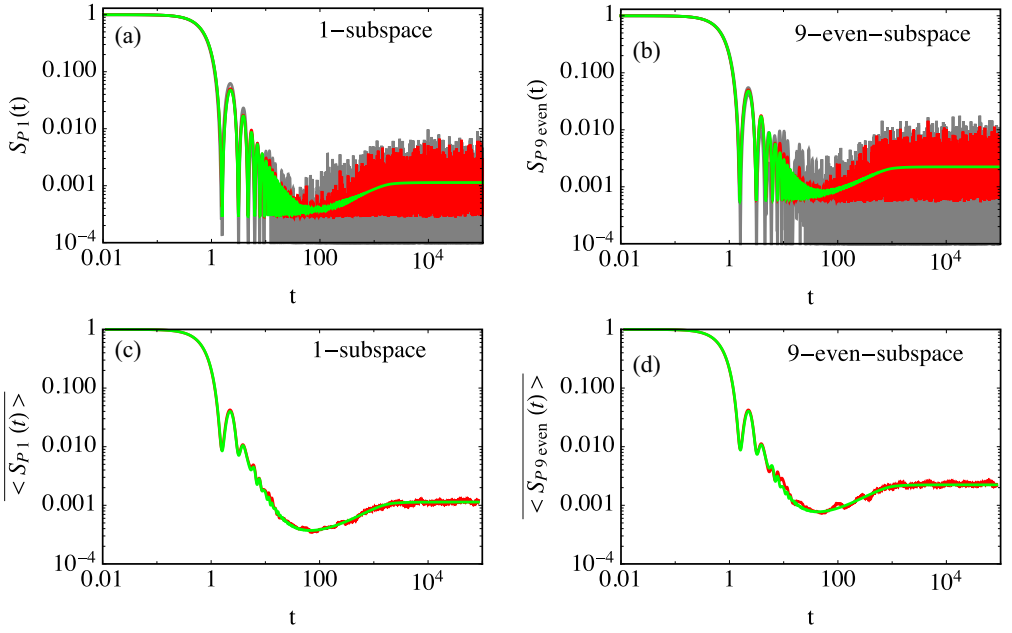

FIG. 4. Survival probability as a function of time in log-log scale. Panels (a) and (b) show, for subspace $j = 1$ and $j = 9$-even, respectively, the survival probability for individual members of the ensemble (gray lines), dark red lines represent the ensemble averages and light green lines are obtained from the analytical Eq. (15). A similar behavior (not shown) was found for the rest of symmetry subspaces. Panels (c) and (d) show averages over temporal windows of constant size in log scale plotted versus the mean time of the respective temporal windows for the numerical ensemble average of $S_P(t)$ (dark red) and for the analytical expression of the survival probability (light green). Panel (c) is for the 1-subspace and panel (d) for the 9-even-subspace.

A. Correlation hole for an ensemble of initial states in the same symmetry subspace

In Fig. 4 we compare numerical results for the survival probability with the analytical expression given by Eq. (15). We employ the same distribution of random initial states in the energy interval $[E_c - \sigma, E_c + \sigma]$ indicated by light-gray columns at the center of the DoS in Fig. 2. For each κ_j subspace, we consider as many random initial states as the number of energy levels of that subspace in the energy interval, i.e, ∼1170 for the $j = 1$–4-subspaces and ∼590 initial states for the subspaces 9-even and 9-odd. The exact numbers are shown in the third column of Table I.

TABLE I. Parameters of the analytical Eq. (15) plotted in Fig. 4 for the $j = 1$ and 9-even-subspaces. Second and third columns come, respectively, from Eqs. (17) and (16). Fourth column is the numerically evaluated mean density of states in the energy window $[E_c - \sigma_R, E_c + \sigma_R]$. Last row shows the parameters used in the analytical Eq. (21) plotted in the top panel of Fig. 7. Second and third-column values come from Eqs. (22) and (16). For the cases shown the parameter η coincides with the respective number of states in the energy window shown by light gray columns in Fig. 2.

j-subspace	$\langle S_P^\infty \rangle \times 10^3$	η	$\overline{\nu}$
1, 8	1.11	1174	293.5
2, 7	1.13	1175	293.7
3, 6	1.13	1178	294.5
4, 5	1.13	1179	294.7
9 even	2.23	597	149.25
9 odd	2.32	574	143.5
Complete	0.210	10581	2645.25

In Figs. 4(a) and 4(b), the gray lines show the survival probability as a function of time for different random initial states with components in the indicated κ_j-subspace, the red lines are the numerical averages over the ensemble, whereas the green line is the analytic expression given in Eq. (15) with parameters determined from Eqs. (16) and (17). We can see that the analytical expression properly describes the temporal trend of the numerical ensemble average. At short times and before the $S_P(t)$ attains its minimum value, the fluctuations of the numerical ensemble average are small, which is a consequence of the fact that the initial decay is determined entirely by the smoothed energy profile of the initial states, Eq. (9), which is the same for every member of the ensemble. At the temporal scale of the correlation hole and beyond, the fluctuations in the numerical ensemble average are relatively larger. To further reduce these fluctuations we consider averages over temporal windows of constant size in log scale. By considering the same smoothing procedure in the analytical expression, we obtain Figs. 4(c) and 4(d), which show an excellent agreement between the analytical expression and numerical averages, and make evident the correlation hole, confirming the existence of a GOE correlated spectrum and thus quantum chaos in this energy region of the Bose-Hubbard model.

1. Survival probability for different regions of the spectrum

In the previous section we have analyzed initial states with random components in the central region of the spectrum. Now we study what happens with the survival probability if we select initial states in energy regions approaching the

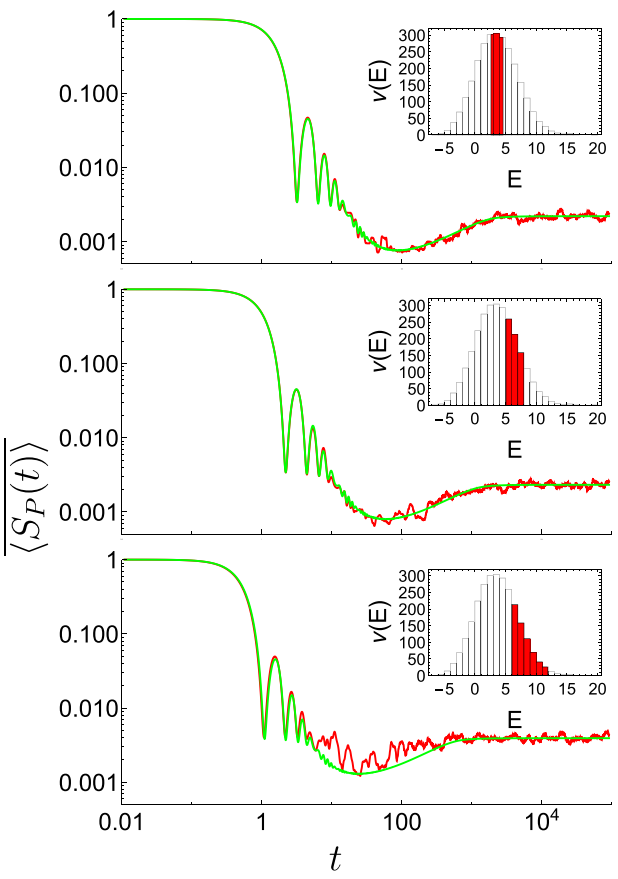

FIG. 5. Averages over temporal window of constant size in log scale of the numerical ensemble average of the Survival probability, plotted versus the mean value of the respective temporal windows (red dark line). Three ensembles over energy regions with 600 levels each were considered. The energy regions of each ensemble are indicated in the histograms shown as insets. Light green lines indicate the same temporal averages of the analytical Eq. (15). Only energy levels of the $j = 1$-subspace were considered. From top to bottom the energy regions move from the center of the spectrum to its highest border.

border of the spectrum. It is known that the universal statistical properties of the chaotic spectra are not applicable to the borders of the spectra, which are model dependent [4]. This is confirmed in the behavior of the survival probability shown in Fig. 5 with dark red lines. Results for three ensembles are shown, one ensemble, as before and used as reference, is located in the center of the DoS and the other two approach the high energy border of the spectrum. We consider again rectangular energy profiles, and move the energy window to the large energy regions using eigenstates of the 1-subspace. The energy windows we consider are shown in the insets of Fig. 5. The number of energy levels contained in the three energy windows is equal to 600.

We observe, as in Fig. 4, a correlation hole for the first and second ensemble of states, located, respectively, in the central part of the spectrum and in a region with slightly higher energies. In both cases the survival probability and correlation hole are very well described by the analytical Eq. (15), shown with light green lines. Since these two ensembles prove energy levels far enough of the borders of the spectrum, the universal behavior expected from the GOE ensemble is clearly observed.

For the third ensemble, located close to the border of the spectrum, we can observe a clear deviation respect to the universal behavior indicated by the light green line obtained from Eq. (15). We observe a correlation hole in the numerical results that is smaller than the one coming from the analytical expression. This implies that, contrary to the two previous ensembles, only a fraction of levels in this energy region have GOE correlations. The participation, in this third ensemble, of energy levels located in the higher part of the spectrum, not only diminish the depth of the correlation hole, but also produce larger oscillations in the survival probability, as can be observed in the bottom panel of Fig. 5.

2. Survival probability for different Hamiltonian parameters

Above we have analyzed the properties of the spectrum of the BHM in the chaotic regime with parameter $u = 0.5$. In this section we study the survival probability with initial states in the same central region of the spectrum of the symmetry sector κ_1, but now for values of the parameter u approaching the integrable limit $u = 0$.

In Fig. 6 we show the combined ensemble and temporal average of the survival probability, both numerical (red) and analytical (green), for four different values of the u parameter. For $u = 0.3$, Fig. 6(a) shows a perfect match between numerical and analytical results and a clear presence of the correlation hole. This is consistent with the nearest-neighbor energy distribution shown in the inset, which is very well described by the Wigner-Dyson surmise. As we approach the integrable limit, the nearest-neighbor energy differences histograms in the insets of Figs. 6(b), 6(c) and 6(d) show that the spectrum correlations disappear. Accordingly, except for the initial decay and asymptotic value, the analytical expression no longer describes the numerical survival probability and instead of a correlation hole we observe revivals whose amplitude increases as the value of u approaches the integrable limit.

B. Correlation hole for an ensemble of initial states in the full space

In this section we present numerical and analytical results for random initial states but considering now the whole set of symmetry sectors. The combined temporal and ensemble average of $S_P(t)$ for a such set of initial states with the participation of levels in the energy interval indicated by light-gray bars in Fig. 2 is shown with a red line in Fig. 7 (top). The important finding is that, even if we employ the complete energy spectrum without any consideration about symmetries, the survival probability exhibits a clearly visible correlation hole, which is again very well described by the analytical expression (green line), now given by Eq. (21), whose parameters shown in Table I are determined from Eqs. (16) and (22).

By inspecting Eq. (21), we observe that the correlation hole is governed mainly by the first term with the two-level form factor b_2 coming from the subspaces $\kappa_j = \kappa_1, ..., \kappa_8$, which is 16 times larger than the second term with the b_2 function coming from the subspaces 9-even and 9-odd. The

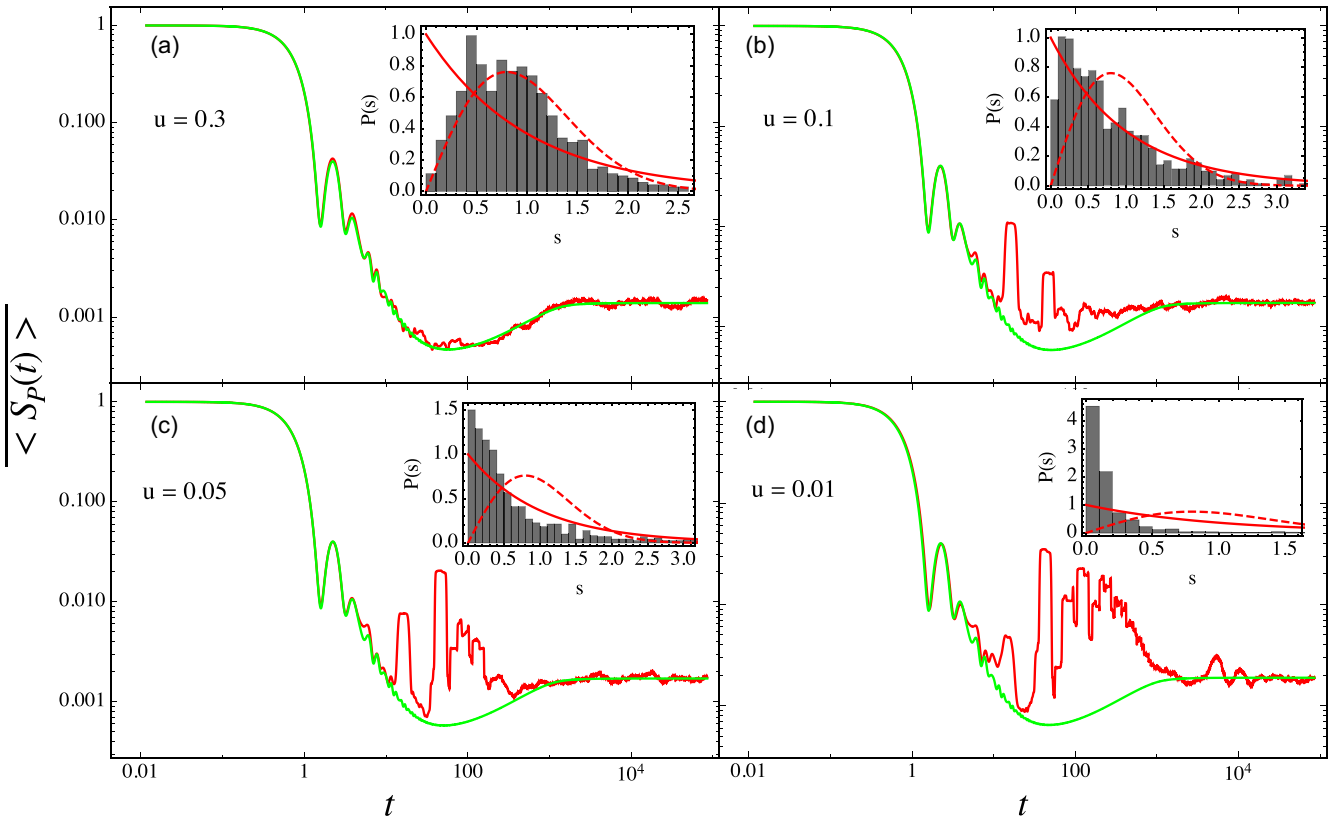

FIG. 6. Averages over temporal windows of the survival probability for initial states with components in the central part of the spectrum of the 1-subspace. The dark red curve is the numerical ensemble average of the survival probability, while the light green line is the analytical Eq. (15). Four different couplings u, indicated in each panel, were used. The insets display the corresponding nearest-neighbor spacing distribution, where the continuous red line is the Poisson distribution and the dashed line is the Wigner-Dyson distribution.

presence of $(L-2)/2$ (for even L) or $(L-1)/2$ (for odd L) sequences of energy levels with similar densities and GOE intra-correlations, is the general scenario that can be found in the BHM for an arbitrary number of sites, and therefore no-exception can be foreseen for the appearance of the correlation hole in the chaotic regime of the BHM for arbitrary size. To illustrate the generality of the previous scenario, we show in Fig. 7 (middle) the same analysis as before, but now for a coupling $u = 0.3$. We observe a perfect match between analytical and numerical results, allowing to conclude that this coupling corresponds also to a chaotic regime.

Finally, in the bottom panel of Fig. 7 we present the survival probability for a coupling, $u = 0.1$, close to the integrable limit. Similarly to the results shown in Figs. 6(b), 6(c) and 6(d), only the initial decay and asymptotic value are well described by the analytical expression. At the temporal scale where the correlation hole would develop, the numerical results show instead partial revivals, indicating that for this coupling there are no GOE correlations even for states belonging to the same symmetry sector.

Figure 7 shows that for an spectrum coming from different symmetry sectors, the correlation hole in the survival probability serves as a good indicator of quantum chaos, differently to the nearest-neighbour-energy differences distribution, which, as shown in the insets of Fig. 7, are Poisson-like in the three cases and thus useless to distinguish a chaotic from a regular regime.

Even in more general chaotic cases, distinct to the BHM, the analytical general formula for the ensemble average of S_P in Eq. (19) and derived in the Appendix, shows that the correlation hole is a general feature appearing in the evolution of the $S_P(t)$ and can be used as a reliable indicator of quantum chaos without having to classify the energy levels according to their symmetries. Additionally, there is no need for unfolding the spectrum, it is a dynamical indicator of chaos useful for experiments that cannot access eigenvalues or eigenstates, and it is a true detector of spectral correlations, contrary to the out-of-time-ordered correlator OTOC which detects instability, not necessarily chaos [44,45].

In this context, it is appropriate to mention a recent study of the temporal evolution of the Survival Probability in the chaotic region of the Dicke model [46], where initial states mixing two subspaces with different parity symmetries are considered. In that reference is also reported the need to employ the full effective dimension η, but only the density of states of every subspace to describe analytically the presence of the correlation hole in the numerical averages. This result is a particular case of the general Eq. (19) for the survival probability when several symmetry subspaces are included.

V. CONCLUSIONS

In the present work we studied dynamical signatures of quantum chaos in the Bose-Hubbard model in a ring configuration. When levels in the same subspace of the shift

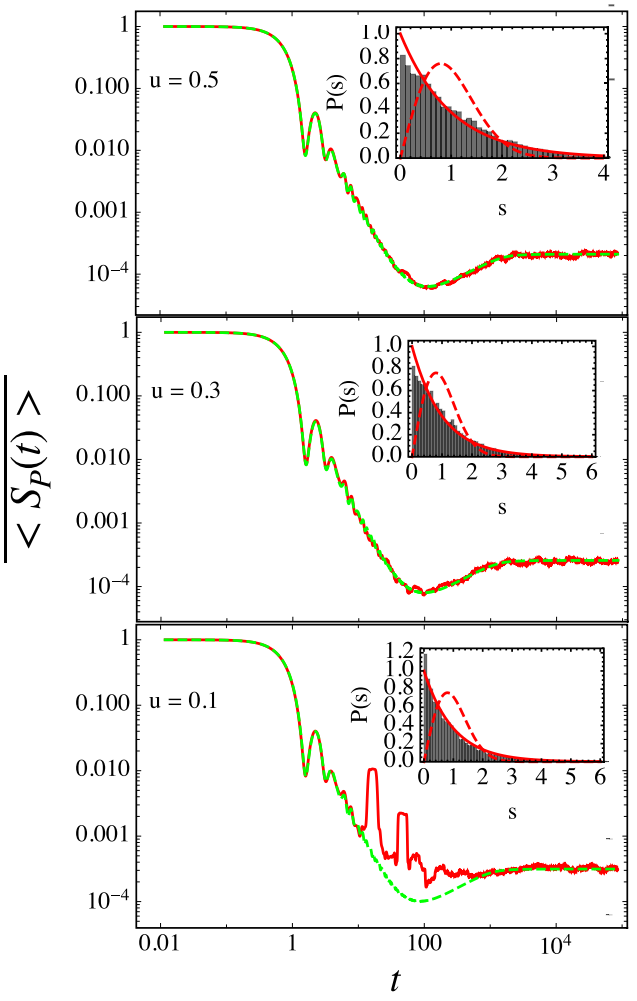

FIG. 7. Dark red lines show rolling temporal averages of the survival probability for the ensemble average of 10 581 initial states with the same number of components inside the central energy interval of all the symmetry subspaces. Three different couplings u, indicated in each panel, were employed. For the top panel the energy interval used is indicated by light-gray bars in panel (a) of Fig. 2. Light green lines are the saem rolling temporal averaged of the analytical expression in Eq. (21). Insets show the corresponding nearest-neighbor spacing distribution of energy levels considering only subspaces $j = 1 - 4$ and $j = 9$.

symmetry are considered, the unfolded nearest-neighbor distribution match the Wigner-Dyson surmise of the Gaussian orthogonal ensemble; however, this is not the case when the full spectrum is included. Nevertheless, for initial states with energies away from the borders of the spectrum, we showed that the ensemble average of the survival probabililty $\langle S_P(t)\rangle$ reveals the presence of spectral correlations by developing a correlation hole, irrespective of whether the initial states are defined over one or several symmetry subspaces. Analytical expressions deduced employing random matrix theory were shown to describe very well the complete evolution of the ensemble average of the survival probability.

Unlike the well established spectral analysis, we found that the correlation hole is a signature of quantum chaos that does not require the classification of energy levels according to their symmetries. Contrary to the analysis of the nearest-neighbor-energy-spacings, in the survival probability the intracorrelations of levels in the same symmetry sectors are not washed out by the absence of correlations between levels coming from different symmetry sectors. The analytical expressions describing perfectly the numerical results were shown to support this claim. The existence of the correlation hole was also related with the presence of quantum chaos for different values of the interaction parameter u.

The fact that the correlation hole is present even when no separation in symmetries is performed, demonstrates that the survival probability is a powerful tool to identify the presence of quantum chaos in systems where the identification of all symmetry sectors may be far from trivial theoretically or experimentally. The correlation hole increases the number of available tools [47,48] to diagnose quantum-chaos without a complete symmetry classification of the energy levels.

An interesting extension of the studies presented here would be to investigate the dynamics of special sets of initial states, like Fock states. The evolution of the survival probability as the dimension of the system changes as well as the study of other observables would be directions worth to be investigated.

ACKNOWLEDGMENTS

We thank L. Santos for the careful reading of the manuscript and her valuable comments, and J. Torres for his useful comments. We acknowledge the support of the Computation Center-ICN, in particular to Enrique Palacios, Luciano Díaz, and Eduardo Murrieta. We acknowledge funding from Mexican Conacyt Project No. CB2015-01/255702, and Crossref is Dirección General de Asuntos del Personal Académico, Universidad Nacional Autónoma de México (DGAPA-UNAM) Projects No. IN109417 and No. IN104020.

APPENDIX: ENSEMBLE AVERAGE OF THE SURVIVAL PROBABILITY FOR SEVERAL DEGENERATE SEQUENCES OF ENERGY LEVELS

Here we generalize the analytical expression for the ensemble average of the survival probability in chaotic regimes derived in Ref. [37] to the case of several symmetry sectors with energy degeneracies, which is the general case of the Bose-Hubbard model.

Let N_e be the number of energy sequences. We assume that the unfolded energies in every sequence have the same correlations as the Gaussian orthogonal ensemble, and no correlations exist between energies of different sequences. Let d_i, ν_i and L_i be, respectively, the degree of degeneracy of each energy level, the density of states and the number of energy levels in the ith energy sequence ($i = 1, ..., N_e$). The following relation holds $\sum_i^{N_e} d_i \nu_i = \nu$, where ν is the density of states of the whole spectrum. The survival probability can be expressed as $S_P(t) = S_P^{\infty} + S_f(t)$ with

$$S_P^{\infty} = \sum_{i=1}^{N_e} \sum_{k=1}^{L_i} \left(\sum_{m=1}^{d_i} \left| c_{ik}^{(m)} \right|^2 \right)^2 \tag{A1}$$

and

$$S_f(t) = \sum_{\substack{i,k,m,i',k',m' \\ (i,k)\neq(i',k')}} \left|c_{ik}^{(m)}\right|^2 \left|c_{i'k'}^{(m')}\right|^2 e^{-i(E_{ik}-E_{i'k'})t}, \tag{A2}$$

where $c_{ik}^{(m)}$ are the energy components of the initial state $|\Psi_o\rangle = \sum c_{i,k}^{(m)} |E_{i,k}; m\rangle$. The term $S_f(t)$ has an infinite temporal average equal to zero, consequently, the first term (S_P^∞) gives the asymptotic value of the survival probability.

As stated in the main text, the components of the initial states are chosen randomly according to

$$\left|c_{ik}^{(m)}\right|^2 = \frac{r_{ik}^{(m)} f(E_{ik})}{\sum_{i'k'm'} r_{i'k'}^{(m')} f(E_{i'k'})},$$

where $f(E_{ik}) = \rho(E_{ik})/\nu(E_{ik})$ and $r_{ik}^{(m)}$ are positive random numbers from a probability distribution $p(r)$.

To derive an analytical expression for the ensemble average of the Survival probability, we proceed similarly as in Ref. [37], and consider the following approximations for the ensemble averages

$$\left\langle \left|c_{ik}^{(m)}\right|^4 \right\rangle \approx \frac{\langle r^2\rangle}{\langle r\rangle^2} f_{ik}^2 \tag{A3}$$

and

$$\left\langle \left|c_{ik}^{(m)}\right|^2 \left|c_{i'k'}^{(m')}\right|^2 \right\rangle \approx \eta \frac{\left(1 - \frac{\langle r^2\rangle}{\langle r\rangle^2}\frac{1}{\eta}\right)}{\eta - 1} f_{ik} f_{i'k'}, \tag{A4}$$

where we have used the shorthand notation $f_{ik} = f(E_{ik})$, $\langle r^n\rangle$ are the nth moments of the probability distribution $p(r)$ and

$$\eta \equiv \frac{1}{\sum_{ikm} f_{ik}^2} \approx \frac{1}{\int \frac{\rho^2(E)}{\nu(E)} dE} \tag{A5}$$

is the effective dimension of states available for the ensemble. In the last equality we have approximated the sum by an integral according to the rule

$$\sum_{i,k,m} G(E_{ik}) \to \int G(E)\nu(E) dE$$

for an arbitrary function $G(E)$.

The previous approximations allow to obtain expressions for the ensemble average of the survival probability and its asymptotic value. For the latter, we consider the RHS of Eq. (A1), expand its squared parenthesis, and take an ensemble average, which upon approximation Eqs. (A3) and (A4), leads to

$$\langle S_P^\infty\rangle_a = \frac{\langle r^2\rangle}{\langle r\rangle^2}\frac{1}{\eta} + \eta \frac{\left(1 - \frac{\langle r^2\rangle}{\langle r\rangle^2}\frac{1}{\eta}\right)}{\eta - 1} \sum_{i=1}^{N_e} d_i(d_i - 1) \sum_{k=1}^{L_i} f_{ik}^2, \tag{A6}$$

where we have used the definition of η in Eq. (A5). The sum over index k in the RHS of the previous equation can be approximated by an integral, but since now the sum is restricted to the ith sequence of energy levels, the density entering in the integral is $\nu_i(E)$:

$$\sum_{k=1}^{L_i} f_{ik}^2 \approx \int \nu_i(E) \left[\frac{\rho(E)}{\nu(E)}\right]^2 dE.$$

By noting that the ratio $\nu_i(E)/\nu(E)$ is a constant, ν_i/ν, the previous integral becomes equal to $\nu_i/(\nu\eta)$, which substituted in Eq. (A6) leads to Eq. (20) of the main text,

$$\langle S_P^\infty\rangle_a = \frac{\langle r^2\rangle}{\langle r\rangle^2}\frac{1}{\eta} + \frac{\left(1 - \frac{\langle r^2\rangle}{\langle r\rangle^2}\frac{1}{\eta}\right)}{\eta - 1} \sum_{i=1}^{N_e} d_i(d_i - 1)\frac{\nu_i}{\nu}. \tag{A7}$$

To obtain an expression for the ensemble average of the entire survival probability, we have to consider now Eq. (A2). The ensemble average of this expression under approximation (A4) yields

$$\langle S_f(t)\rangle = \eta \frac{\left(1 - \frac{\langle r^2\rangle}{\langle r\rangle^2}\frac{1}{\eta}\right)}{\eta - 1} \sum_{\substack{i,k,m,i',k',m' \\ (i,k)\neq(i'k')}} f_{ik} f_{i'k'} e^{-i(E_{ik}-E_{i'k'})t}.$$

To approximate the double sum in the previous expression by a double integral, we have to take into account possible correlations between energy levels. If the energy levels were completely uncorrelated, then the double sum for an arbitrary function $G(E, E')$ could be properly approximated as $\sum_{\alpha,\alpha'} G(E_\alpha, E_{\alpha'}) \to \int dE dE' \nu(E)\nu(E') G(E, E')$, where we have introduced the short-hand notation $\alpha \equiv (i, k, m)$. On the contrary, for correlated energy levels, in addition to the product of densities ν, the two-level cluster function $T(E - E')$ should be included, defining the Dyson two-point correlation function [49],

$$R(E, E') = \nu(E)\nu(E') - T(E - E'),$$

with which the double sum would be approximated as

$$\sum_{\alpha,\alpha'} G(E_\alpha, E_{\alpha'}) \to \int dE dE' R(E, E') G(E, E'). \tag{A8}$$

The case we are handling here mixes both situations: levels coming from different energy sequences are not correlated, whereas levels coming from the same sequence (with degeneracy d_i) have GOE correlations described by a two-level cluster function $T_i(E - E')$. Therefore, the double sum becomes

$$\sum_{\substack{i,k,m,i',k',m' \\ (i,k)\neq(i'k')}} f_{ik} f_{i'k'} e^{-i(E_{ik}-E_{i'k'})t} \longrightarrow$$

$$\int \nu(E)\nu(E') f(E) f(E') e^{-i(E-E')t} dE dE'$$

$$- \sum_{im,i'm'} \delta_{ii'} \int T_i(E - E') f(E) f(E') e^{-i(E-E')t} dE dE'. \tag{A9}$$

Note that in the first integral participate all the energy levels, whereas only correlated levels contribute to the second term. This fact is the key point that allows the survival probability to detect GOE correlations even if different symmetry sectors are considered together.

By recalling that $f(E) = \rho(E)/\nu(E)$, the double integrals in Eq. (A9) simplify to

$$\left|\int \rho(E) e^{-iEt} dE\right|^2$$

$$- \sum_i d_i^2 \int \frac{T_i(E - E')}{\nu(E)\nu(E')} \rho(E)\rho(E') e^{-i(E-E')t} dE dE', \tag{A10}$$

where the squared degeneracies d_i^2 come from the double sum over variables m and m' in Eq. (A9). The ratio $T_i(E-E')/[\nu_i(E)\nu_i(E')]$ defines, in the limit of an infinite number of levels, an universal function in terms of unfolded energies $Y([E-E']\bar{\nu}_i) = T_i(E-E')/[\nu_i(E)\nu_i(E'))]$, where $\nu_i(E)$ is the density of states of the ith sequence and $\bar{\nu}_i$ its mean value in the energy region probed by the ensemble. With this function, the second term in Eq. (A10) can be written as

$$\sum_i d_i^2\left(\frac{\nu_i}{\nu}\right)^2 \int Y([E-E']\bar{\nu}_i)\rho(E)\rho(E')e^{-i(E-E')t}dEdE',$$

where we have used that the ratio $\nu_i(E)/\nu(E)$ becomes independent of E. By making the change of variables $x = (E-E')\bar{\nu}_i$ and $z = E'$, the previous expression reads

$$\sum_i d_i^2\left(\frac{\nu_i}{\nu}\right)^2 \frac{1}{\bar{\nu}_i}\int dzdx\rho(z)\rho(z+x/\bar{\nu}_i)Y(x)e^{-i2\pi x\bar{t}},$$

with $\bar{t} = t/(2\pi\bar{\nu}_i)$. By expanding $\rho(z+x/\bar{\nu}_i)$ in powers of x and considering only the lowest order, the double integral appearing in the previous expression can be approximated by a product of two independent integrals

$$\sum_i d_i^2\left(\frac{\nu_i}{\nu}\right)^2 \frac{1}{\bar{\nu}_i}\int dz\rho(z)^2\int dxY(x)e^{-i2\pi x\bar{t}} = \frac{1}{\eta}\sum_i d_i^2\frac{\bar{\nu}_i}{\bar{\nu}}b_2\left(\frac{t}{2\pi\bar{\nu}_i}\right), \tag{A11}$$

where we have used $\nu_i/\nu = \bar{\nu}_i/\bar{\nu}$, the definition of η in Eq. (A5) and b_2 is the known Fourier transform of the GOE two-level cluster function $Y(x)$ [49], the so called two-level form factor shown in Eq. (18). Gathering the previous results together, we obtain the expression for the ensemble average of the survival probability shown in Eq. (19) of the main text

$$\langle S_P(t)\rangle_a = \frac{\left(1-\frac{\langle r^2\rangle}{\langle r\rangle^2}\frac{1}{\eta}\right)}{\eta-1} \times\left[\eta S_P^{bc}(t) - \sum_{i=1}^{N_e} d_i^2\frac{\bar{\nu}_i}{\bar{\nu}}b_2\left(\frac{t}{2\pi\bar{\nu}_i}\right)\right] + \langle S_P^{\infty}\rangle_a, \tag{A12}$$

where $S_P^{bc}(t) = |\int\rho(E)e^{-iEt}dE|^2$ gives the initial decay of the survival probability and $\langle S_P^{\infty}\rangle_a$ is given in Eq. (A7). It is straightforward to show that the previous expression for the survival probability has the right value in $t=0$, $\langle S_P(t=0)\rangle_a = 1$.

For the Bose-Hubbard model we consider in this paper ($L=N=9$), we have six sequences of energy levels, four of them have degeneracy two ($d_1=d_2=d_3=d_4=2$) and the other two are nondegenerate $d_{9\text{-even}} = d_{9\text{-odd}} = 1$. The respective density of states are $\nu_1=\nu_2=\nu_3=\nu_4=\nu/9$ and $\nu_{9\text{-even}} = \nu_{9\text{-odd}} = \nu/18$. For this case, the ensemble averages read

$$\langle S_P^{\infty}\rangle_a = \frac{\langle r^2\rangle}{\langle r\rangle^2}\frac{1}{\eta} + \frac{\left(1-\frac{\langle r^2\rangle}{\langle r\rangle^2}\frac{1}{\eta}\right)}{\eta-1}\frac{8}{9} \tag{A13}$$

and

$$\langle S_P(t)\rangle = \langle S_P^{\infty}\rangle_a + \frac{\left(1-\frac{\langle r^2\rangle}{\langle r\rangle^2}\frac{1}{\eta}\right)}{\eta-1} \times\left[\eta S_P^{bc}(t) - \frac{16}{9}b_2\left(\frac{9t}{2\pi\bar{\nu}}\right) - \frac{1}{9}b_2\left(\frac{9t}{\pi\bar{\nu}}\right)\right]. \tag{A14}$$

For the particular uniform distribution $p(r)$ we consider in the main text $\frac{\langle r^2\rangle}{\langle r\rangle^2} = \frac{4}{3}$. By substituting this ratio in Eqs. (A13) and (A14) we retrieve Eqs. (21) and (22) of the main text.

[1] J. von Neuman and E. P. Wigner, Uber das Verhalten von Eigenwerten bei adiabatischen Prozessen, Phys. Zschr. **30**, 294 (1929).

[2] L. Reichl, *The Transition to Chaos: Conservative Classical Systems and Quantum Manifestations* (Springer Science & Business Media, Berlin, 2013).

[3] H. J. Stöckmann, *Quantum Chaos: An Introduction*, Quantum Chaos: An Introduction (Cambridge University Press, Cambridge, UK, 2006).

[4] M. C. Gutzwiller, *Chaos in Classical and Quantum Mechanics*, Vol. 1 (Springer Science & Business Media, Berlin, 2013).

[5] M. V. Berry, M. Tabor, and J. M. Ziman, Level clustering in the regular spectrum, Proc. R. Soc. London A **356**, 375 (1977).

[6] O. Bohigas, M. J. Giannoni, and C. Schmit, Characterization of Chaotic Quantum Spectra and Universality of Level Fluctuation Laws, Phys. Rev. Lett. **52**, 1 (1984).

[7] I. C. Percival, Regular and irregular spectra, J. Phys. B: At. Mol. Phys. **6**, L229 (1973).

[8] M. Greiner, O. Mandel, T. Esslinger, T. W. Hänsch, and I. Bloch, Quantum phase transition from a superfluid to a Mott insulator in a gas of ultracold atoms, Nature **415**, 39 (2002).

[9] W. S. Bakr, J. I. Gillen, A. Peng, S. Fölling, and M. Greiner, A quantum gas microscope for detecting single atoms in a Hubbard-regime optical lattice, Nature **462**, 74 (2009).

[10] W. S. Bakr, A. Peng, M. E. Tai, R. Ma, J. Simon, J. I. Gillen, S. Fölling, L. Pollet, and M. Greiner, Probing the superfluid–to–Mott insulator transition at the single-atom level, Science **329**, 547 (2010).

[11] R. Islam, R. Ma, P. M. Preiss, M. E. Tai, A. Lukin, M. Rispoli, and M. Greiner, Measuring entanglement entropy in a quantum many-body system, Nature **528**, 77 (2015).

[12] A. M. Kaufman, M. E. Tai, A. Lukin, M. Rispoli, R. Schittko, P. M. Preiss, and M. Greiner, Quantum thermalization through entanglement in an isolated many-body system, Science **353**, 794 (2016).

[13] A. Lukin, M. Rispoli, R. Schittko, M. E. Tai, A. M. Kaufman, S. Choi, V. Khemani, J. Léonard, and M. Greiner, Probing entanglement in a many-body–localized system, Science **364**, 256 (2019).

[14] J. Cotler, S. Choi, A. Lukin, H. Gharibyan, T. Grover, M. E. Tai, M. Rispoli, R. Schittko, P. M. Preiss, A. M. Kaufman, M.

Greiner, H. Pichler, and P. Hayden, Quantum Virtual Cooling, Phys. Rev. X **9**, 031013 (2019).
[15] A. R. Kolovsky and A. Buchleitner, Quantum chaos in the Bose-Hubbard model, Europhys. Lett. **68**, 632 (2004).
[16] M. Lubasch, Quantum chaos and entanglement in the Bose-Hubbard model, Master thesis, Heidelberg University, 2009, https://www.thphys.uni-heidelberg.de/∼wimberger/ma_lubasch.pdf.
[17] T. Engl, J. Dujardin, A. Argüelles, P. Schlagheck, K. Richter, and J. D. Urbina, Coherent Backscattering in Fock Space: A Signature of Quantum Many-Body Interference in Interacting Bosonic Systems, Phys. Rev. Lett. **112**, 140403 (2014).
[18] T. Engl, J. D. Urbina, and K. Richter, Periodic mean-field solutions and the spectra of discrete bosonic fields: Trace formula for Bose-Hubbard models, Phys. Rev. E **92**, 062907 (2015).
[19] A. R. Kolovsky, Bose–Hubbard Hamiltonian: Quantum chaos approach, Int. J. Mod. Phys. B **30**, 1630009 (2016).
[20] H. Shen, P. Zhang, R. Fan, and H. Zhai, Out-of-time-order correlation at a quantum phase transition, Phys. Rev. B **96**, 054503 (2017).
[21] R. A. Kidd, M. K. Olsen, and J. F. Corney, Quantum chaos in a Bose-Hubbard dimer with modulated tunneling, Phys. Rev. A **100**, 013625 (2019).
[22] A. Russomanno, M. Fava and R. Fazio, Non-ergodic behavior of clean Bose-Hubbard chains, arXiv:2005.09892.
[23] J. P. Pique, Y. Chen, R. W. Field and J. L. Kinsey, Chaos and Dynamics on 0.5–300 ps Timescales in Vibrationally Excited Acetylene: Fourier Transform of Stimulated-Emission Pumping Spectrum, Phys. Rev. Lett. **58**, 475 (1987).
[24] A. Delon, R. Jost, and M. Lombardi, NO_2 jet cooled visible excitation spectrum: Vibronic chaos induced by the X^2A_1–A^2B_2 interaction, J. Chem. Phys. **95**, 5701 (1991).
[25] M. Lombardi and T. H. Seligman, Universal and nonuniversal statistical properties of levels and intensities for chaotic Rydberg molecules, Phys. Rev. A **47**, 3571 (1993).
[26] L. Michaille and J.-P. Pique, Influence of Experimental Resolution on the Spectral Statistics Used to Show Quantum Chaos: The Case of Molecular Vibrational Chaos, Phys. Rev. Lett. **82**, 2083 (1999).
[27] T. Guhr and H. A. Weidenmüller, Correlations in anticrossing spectra and scattering theory. Analytical aspects, Chem. Phys. **146**, 21 (1990).
[28] J. Wilkie and P. Brumer, Time-Dependent Manifestations of Quantum Chaos, Phys. Rev. Lett. **67**, 1185 (1991).
[29] U. Hartmann, H. A. Weidenmüller, and T. Guhr, Correlations in anticrossing spectra and scattering theory: Numerical simulations, Chem. Phys. **150**, 311 (1991).
[30] Y. Alhassid and R. D. Levine, Spectral autocorrelation function in the statistical theory of energy levels, Phys. Rev. A **46**, 4650 (1992).
[31] G. Casati, I. Guarneri, and G. Mantica, Random matrices as models for the statistics of quantum mechanics, Physica D **21**, 105 (1986).
[32] E. J. Torres-Herrera and L. F. Santos, Extended nonergodic states in disordered many-body quantum systems, Annalen der Physik **529**, 1600284 (2017).
[33] E. J. Torres-Herrera and L. F. Santos, Dynamical manifestations of quantum chaos: Correlation hole and bulge, Philos. Trans. R. Soc. London A **375**, 20160434 (2017).
[34] E. J. Torres-Herrera, A. M. García-García, and L. F. Santos, Generic dynamical features of quenched interacting quantum systems: Survival probability, density imbalance, and out-of-time-ordered correlator, Phys. Rev. B **97**, 060303 (2018).
[35] E. J. Torres-Herrera and L. F. Santos, Signatures of chaos and thermalization in the dynamics of many-body quantum systems, Eur. Phys. J.: Spec. Top. **227**, 1897 (2019).
[36] M. Schiulaz, E. J. Torres-Herrera, and L. F. Santos, Thouless and relaxation timescales in many-body quantum systems, Phys. Rev. B **99**, 174313 (2019).
[37] S. Lerma-Hernández, D. Villaseñor, M. A. Bastarrachea-Magnani, E. J. Torres-Herrera, L. F. Santos, and J. G. Hirsch, Dynamical signatures of quantum chaos and relaxation time scales in a spin-boson system, Phys. Rev. E **100**, 012218 (2019).
[38] E. J. Torres-Herrera, G. De Tomasi, M. Schiulaz, F. Pérez-Bernal, L. F. Santos, Self-averaging in many-body quantum systems out of equilibrium, II. Approach to the localized phase, arXiv:1910.11332.
[39] M. Schiulaz, E. J. Torres-Herrera, F. Pérez-Bernal, and L. F. Santos, Self-averaging in many-body quantum systems out of equilibrium: Chaotic systems, Phys. Rev. B **101**, 174312 (2020).
[40] D. Yang, A. Grankin, L. M. Sieberer, D. V. Vasilyev, and P. Zoller, Quantum non-demolition measurement of a many-body Hamiltonian, Nat. Commun. **11**, 775 (2020).
[41] M. P. A. Fisher, P. B. Weichman, G. Grinstein, and D. S. Fisher, Boson localization and the superfluid-insulator transition, Phys. Rev. B **40**, 546 (1989).
[42] F. M. Cucchietti, B. Damski, J. Dziarmaga, and W. H. Zurek, Dynamics of the Bose-Hubbard model: Transition from a Mott insulator to a superfluid, Phys. Rev. A **75**, 023603 (2007).
[43] A. R. Kolovsky and A. Buchleitner, Floquet-Bloch operator for the Bose-Hubbard model with static field, Phys. Rev. E **68**, 056213 (2003).
[44] Q. Hummel, B. Geiger, J. D. Urbina, and K. Richter, Reversible Quantum Information Spreading in Many-Body Systems Near Criticality, Phys. Rev. Lett. **123**, 160401 (2019).
[45] S. Pilatowsky-Cameo, J. Chávez-Carlos, M. A. Bastarrachea-Magnani, P. Stránský, S. Lerma-Hernández, L. F. Santos, and J. G. Hirsch, Positive quantum Lyapunov exponents in experimental systems with a regular classical limit, Phys. Rev. E **101**, 010202(R) (2020).
[46] D. Villaseñor, S. Pilatowsky-Cameo, M. A. Bastarrachea-Magnani, S. Lerma-Hernández, L. F. Santos, and J. G. Hirsch, Quantum vs. classical dynamics in a spin-boson system: Manifestations of spectral correlations and scarring, New J. Phys. **22**, 063036 (2020).
[47] E. M. Fortes, I. García-Mata, R. A. Jalabert, and D. A. Wisniacki, Gauging classical and quantum integrability through out-of-time-ordered correlators, Phys. Rev. E **100**, 042201 (2019).
[48] M. Pandey, P. W. Claeys, D. K. Campbell, A. Polkovnikov, and D. Sels, Adiabatic eigenstate deformations as a sensitive probe for quantum chaos, arXiv:2004.05043.
[49] M. L. Mehta, *Random Matrices* (Academic Press, Boston, MA, 1991).